Theoretical and matrix isolation FTIR studies of 3-amino-1,2,4-triazole and its isomers

ARTICLE *in* CHEMICAL PHYSICS LETTERS · MAY 2009

Impact Factor: 1.9 · DOI: 10.1016/j.cplett.2009.03.079

3 AUTHORS, INCLUDING:

Magdalena Pagacz-Kostrzewa
University of Wroclaw
9 PUBLICATIONS **60** CITATIONS
SEE PROFILE

Maria Wierzejewska
University of Wroclaw
61 PUBLICATIONS **475** CITATIONS
SEE PROFILE

Chemical Physics Letters 473 (2009) 238–246

Contents lists available at ScienceDirect

Chemical Physics Letters

journal homepage: www.elsevier.com/locate/cplett

Theoretical and matrix isolation FTIR studies of 3-amino-1,2,4-triazole and its isomers

Magdalena Pagacz-Kostrzewa, Robert Bronisz, Maria Wierzejewska*

Faculty of Chemistry, University of Wrocław, Joliot-Curie 14, 50-383 Wrocław, Poland

ARTICLE INFO

Article history:
Received 11 March 2009
In final form 30 March 2009
Available online 2 April 2009

ABSTRACT

The structure, isomerization pathways and vibrational spectra of the important heterocyclic 3-amino-1,2,4-triazole (AT) molecule were studied by MP2 and B3LYP methods. Among 11 minima located on PES, 3-amino-1,2,4-*1H*-triazole (1-AT) and 3-amino-1,2,4-*2H*-triazole (2-AT) are the most stable with the calculated abundance at 298 K of 79.4% and 20.6%, respectively. The presented FTIR results allow unequivocal identification and characterization of two AT tautomers isolated in an argon matrix. The performed studies reveal that conformational cooling does not take place in the studied matrices. This observation is consistent with the predicted high energy barrier of ca. 45 kcal/mol for a direct 1,2-hydrogen transfer between 1-AT and 2-AT species.

1. Introduction

Triazoles and their derivatives belong to one of the most important heterocyclic family. The literature concerning the 1,2,3- and 1,2,4-triazoles is rich and the papers published cover such subjects as crystal structure determination [1,2], ab initio and DFT calculations on the tautomerism and protonation sites [3–10], vibrational characteristics and photochemical transformations [11–16] and thermal decomposition products [17–19]. Many reports appeared on the synthesis and characterization of novel triazole containing organic [20–22] or metal coordination compounds [23–26] including spin-crossover materials [27–29].

The title compound, 3-amino-1,2,4-triazole (AT) is a popular nonselective herbicide used on nonfood croplands to control annual grasses, broadleaf and aquatic weeds. It has also a diverse biochemical activity and is used as a reagent for the determination of tryptophan in proteins. Because it has a strong coordination properties, light sensitivity and biological activity, is widely used in synthesis and preparation of the antibiotics, triazole diimine dyes, sensitive materials and plant growth regulator. AT is also interesting itself since it may exhibit the annular tautomerism as well as the amino–imino tautomerism. The X-ray crystal structure of AT [30] shows the presence of the 3-amino-1,2,4-*2H*-triazole conformer. The individual molecules are linked by several different N–H···N hydrogen bonds, with the shortest N···N distance of 2.896 Å.

Here, the results of a systematic search for the possible minima on the potential energy surface of the 3-amino-1,2,4-triazole molecule are reported. We performed also the FTIR matrix isolation studies in the aim to characterize the most stable isomers of AT present in low temperature argon matrices. This technique proved to be a powerful tool for conformational studies [31–33]. Depending on the height of the barriers for intramolecular rearrangement in the studied molecule the gas phase concentration ratio of isomers may be either preserved in low temperature matrices or changed because of the interconversion processes during deposition [34].

2. Experimental

2.1. Computational details

All calculations were performed with the GAUSSIAN 03 program package [35]. Structures of the minima and transition states were optimized at both B3LYP and MP2 levels using the 6-311++G(2d,2p) basis set. The associated force constant matrixes were calculated to evaluate harmonic frequencies and zero-point vibrational (ZPE) corrections. The B3LYP/6-311++G(2d,2p) calculated frequencies were scaled by 0.955 above 2000 cm^{-1} and by 0.977 for the 2000–400 cm^{-1} spectral region. The scaling factors were determined by linear fitting with intercept zero. Potential energy distributions (PED) of the normal modes were computed with the GAR2PED program [36] and the vibrational spectra were simulated using SYNSPEC program [37].

2.2. Matrix isolation studies

In order to obtain matrices containing AT, the crystalline sample was allowed to sublimate at 333 K from a small electric oven located inside the vacuum vessel of the cryostat near the cold window. The temperature of the oven was controlled by the DC

* Corresponding author. Fax: +48 71 3282348.
E-mail address: mariaw@wchuwr.pl (M. Wierzejewska).

0009-2614/$ - see front matter © 2009 Elsevier B.V. All rights reserved.
doi:10.1016/j.cplett.2009.03.079

regulated power supply (NDN Instruments) that allowed for the precise regulation of the current. The vapour of AT were deposited onto a cold CsI window with a large excess of matrix gas. The temperature of the cold window was maintained at a temperature 10–22 K by means of a closed cycle helium refrigerator (ARS-2HW). Infrared spectra were recorded between 4000 and 400 cm^{-1} in a transmission mode with a resolution of 0.5 cm^{-1} by means of a Bruker 66 FTIR spectrometer equipped with a liquid N_2 cooled MCT detector.

A commercially available 3-amino-1,2,4-triazole (Fluka) was purified by column chromatography on silica gel K60 (Merck, 230–400 mesh) using dichloromethane/methanol-9/3(v/v) mixture as an eluent (R_f = 0.63).

3. Results and discussion

3.1. DFT and MP2 calculations: tautomerism and molecular geometries

The optimized structures of the AT minima are presented in Fig. 1 together with the adopted numbering scheme while those obtained for the transition states are shown in Fig. 2. The geometric parameters of three most stable species obtained at the B3LYP/MP2 levels are gathered in Table 1 together with the available experimental values [30]. The selected structural parameters calculated at both levels for eight less stable isomers are gathered in Table S1 in Supplementary material. All species but those which possess planar structures have their mirror-image of the same energy; the latter species will not be considered further.

The related energetics for minima and transition states is given in Tables 2 and 3, respectively. From now on the structures and energies discussed are those from B3LYP/6-311++G(2d,2p) calculations and the MP2/6-311++G(2d,2p) results are given after slash. All energies discussed throughout the paper are those with the zero-point vibrational energy correction (ZPE) included.

Generally, the applied B3LYP and MP2 methods predicted very much the same geometries for both minima and transition states located on the potential energy surface. There are no significant differences in the values of the bond distances and bond angles computed at both levels, with variations of less than 1.7%. Also, the dihedral angles values are fairly independent of the method used.

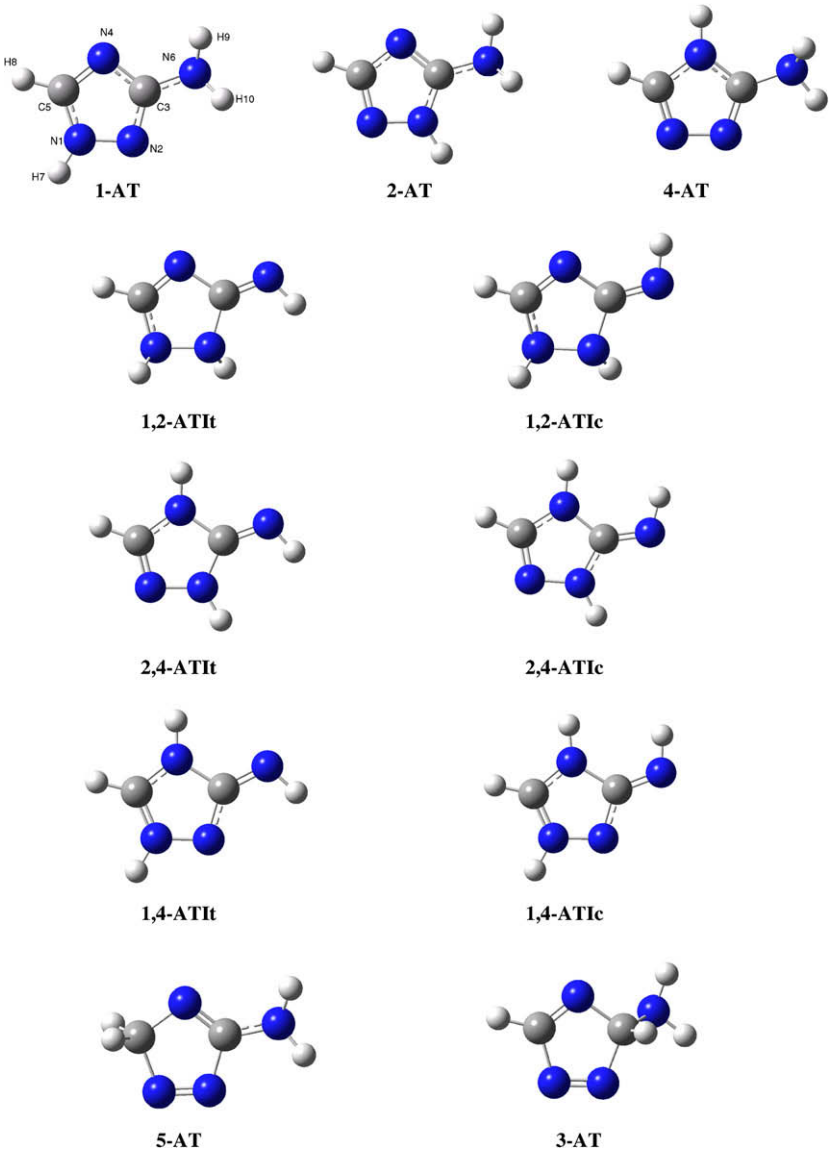

Fig. 1. Optimized structures of the AT isomers.

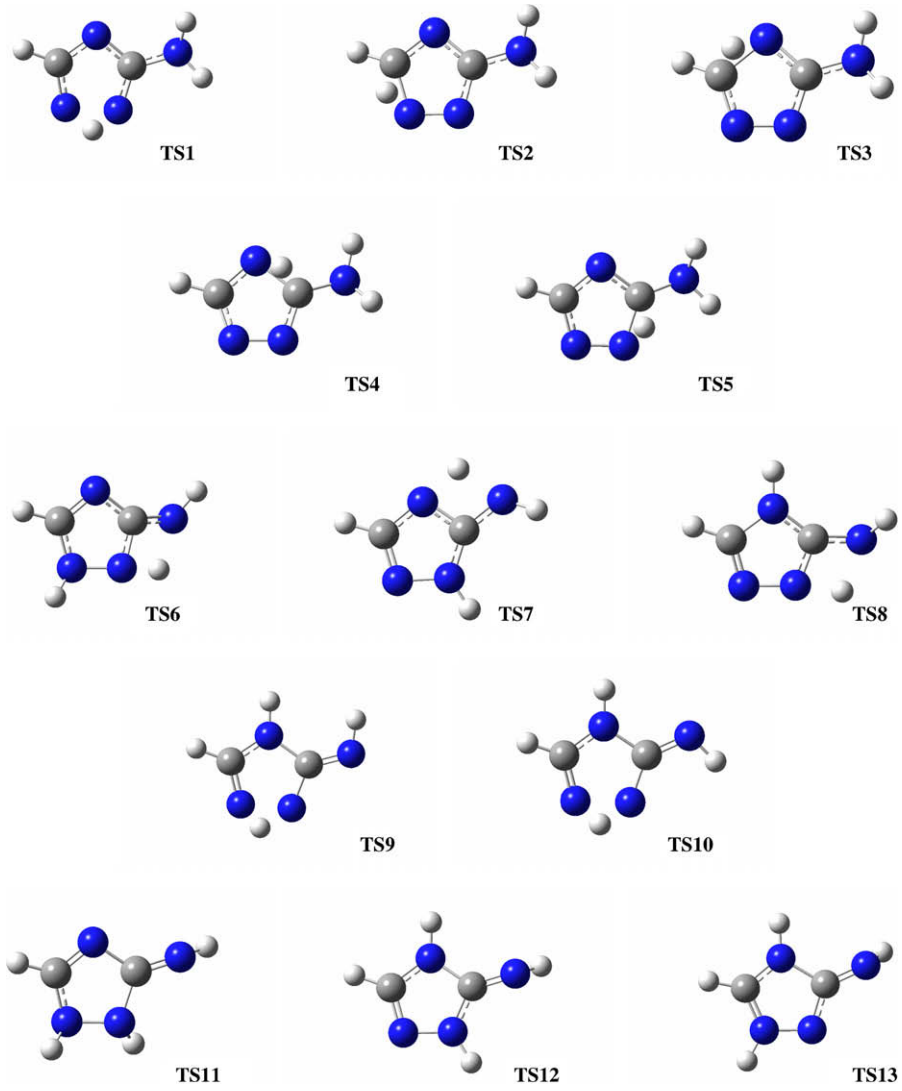

Fig. 2. Optimized structures of the transition states.

Table 1
Selected geometric parameters (Å, deg) calculated at B3LYP/MP2 levels for 1-AT, 2-AT and 4-AT compared to the X-ray experimental data.

Parameter	1-AT	2-AT	4-AT	Exp. 2-AT
R(NH7)	1.004/1.004	1.004/1.004	1.005/1.005	0.86(6)
R(N6H9)	1.007/1.007	1.009/1.008	1.011/1.010	0.89(6)
R(N6H10)	1.007/1.007	1.008/1.008	1.011/1.010	0.92(6)
R(N1N2)	1.367/1.356	1.372/1.360	1.391/1.391	1.378(8)
R(N1C5)	1.340/1.348	1.314/1.331	1.298/1.317	1.311(8)
R(N2C3)	1.325/1.337	1.350/1.352	1.306/1.318	1.340(8)
R(C5N4)	1.318/1.328	1.366/1.367	1.375/1.368	1.362(8)
R(C3N4)	1.366/1.362	1.319/1.324	1.368/1.365	1.340(8)
R(C3N6)	1.379/1.386	1.380/1.391	1.388/1.395	1.342(8)
θ(N2N1C5)	110.2/110.8	101.7/101.5	107.5/107.1	102.6(5)
θ(N1C5N4)	110.2/109.8	115.6/115.3	110.4/110.4	115.0(5)
θ(N1N2C3)	101.6/101.5	109.9/110.6	107.3/107.2	109.8(5)
θ(N2C3N4)	115.0/115.1	109.9/109.8	110.4/110.4	109.4(5)
θ(C3N6H10)	114.4/112.9	115.6/113.6	110.2/109.0	123(4)
θ(C3N6H9)	113.6/112.0	111.7/109.7	114.2/112.8	126(4)
θ(H9N6H10)	113.5/111.9	111.9/109.9	110.2/108.8	107(4)
ϕ(N2C3N6H9)	−156.6/−153.9	−171.2/−178.5	−127.6/−117.4	−174(4)
ϕ(N2C3N6H10)	−23.9/−26.5	−41.7/−55.1	−3.0/3.5	−13(4)
ϕ(N4C3N6H9)	26.4/29.8	12.5/5.8	56.7/67.0	8(4)
ϕ(N4C3N6H10)	159.0/157.2	142.0/129.3	−178.7/−172.0	169(4)

There are two kinds of tautomerism available for the studied AT molecule. First, proton from the NH group can occupy three positions on the ring resulting in the 1H-, 2H- and 4H-tautomers. Second, due to the presence of the NH_2 group in AT the amino–imino tautomersim is possible.

3.1.1. Geometries of the AT amino forms

According to the calculations all three annular tautomers of the AT amino form: 1-AT, 2-AT and 4-AT are predicted to be true minima at both B3LYP and MP2 levels. The most stable is the 1-AT form with the annular H-atom attached to the N1 atom of the triazole ring and the 2-AT tautomer is by 0.89/1.02 kcal/mol higher in energy then 1-AT. The least stable amino form 4-AT is 7.89/7.30 kcal/mol above the global minimum. None of these structures is planar. The N atom of the amino group lies on the triazole ring plane with both H atoms of the NH_2 group sticking out of this plane. The corresponding dihedral angles ϕ($N_2C_3N_6H_9$) and ϕ ($N_4C_3N_6H_{10}$) presented in Table 1 show asymmetry of the NH_2 group relative to the ring plane in the higher energy 2-AT and 4-AT conformers as compared with 1-AT. From the values of these parameters it is clear that the observed effect is related to the repulsive interaction present in the higher energy AT forms

Table 2
Relative Energies, Relative Gibbs Free Energies (kcal/mol) and abundances at 298 and 333 K for AT conformers calculated at the B3LYP and MP2 levels with the 6-311++G(2d,2p) basis set.

Isomer	n[a]	B3LYP/6-311G(2d,2p)					MP2/6-311G(2d,2p)				
		ΔE	ΔE^{ZPE}	ΔG	$\%_{298K}$	$\%_{333K}$	ΔE	ΔE^{ZPE}	ΔG	$\%_{298K}$	$\%_{333K}$
1-AT	2	0.00	0.00	0.00	79.39	78.94	0.00	0.00	0.00	81.89	81.39
2-AT	2	0.93	0.89	0.80	20.61	21.06	0.88	1.02	0.89	18.11	18.61
4-AT	2	8.34	7.89	7.80	0.00	0.00	8.20	7.30	7.19	0.00	0.00
1,2-ATIt	2	25.93	25.76	25.80	0.00	0.00	30.77	30.56	30.59	0.00	0.00
1,2-ATIc	2	22.42	22.40	22.45	0.00	0.00	27.36	27.31	27.36	0.00	0.00
2,4-ATIc	1	13.85	12.93	12.47	0.00	0.00	17.22	16.20	15.86	0.00	0.00
2,4-ATIt	1	13.02	12.16	11.59	0.00	0.00	16.41	15.44	14.99	0.00	0.00
1,4-ATIc	1	35.07	34.08	34.05	0.00	0.00	37.78	36.55	36.50	0.00	0.00
1,4-ATIt	1	29.77	29.12	29.14	0.00	0.00	32.77	31.92	31.94	0.00	0.00
5-AT	2	22.45	21.23	21.16	0.00	0.00	24.54	23.30	23.26	0.00	0.00
3-AT	2	40.04	38.80	38.53	0.00	0.00	39.36	38.06	37.85	0.00	0.00

[a] *n* denotes the degeneracy factor.

Table 3
Relative energies, relative Gibbs free energies (kcal/mol) and imaginary frequencies for transition states calculated at B3LYP and MP2 levels with the 6-311++G(2d,2p) basis set.

	B3LYP/6-311G(2d,2p)				MP2/6-311G(2d,2p)			
	ΔE	ΔE^{ZPE}	ΔG_{298}	v_i	ΔE	ΔE^{ZPE}	ΔG_{298}	v_i
TS1	50.08	46.18	46.21	1711*i*	49.18	45.20	45.25	1632*i*
TS2	51.66	48.09	48.17	1442*i*	52.06	48.46	48.56	1388*i*
TS3	61.25	57.43	57.47	1567*i*	58.74	54.79	54.84	1468*i*
TS4	67.15	63.40	63.40	1441*i*	64.34	60.47	60.47	1372*i*
TS5	60.52	57.01	57.05	1326*i*	59.68	56.11	56.14	1303*i*
TS6	69.53	65.68	65.84	1921*i*	72.43	68.54	68.72	1902*i*
TS7	60.53	56.36	56.23	1933*i*	62.42	58.30	58.32	1905*i*
TS8	66.30	62.14	62.21	1890*i*	66.99	62.77	62.89	1835*i*
TS9	78.45	73.94	73.96	1696*i*	80.57	75.96	76.00	1578*i*
TS10	73.12	68.91	68.94	1677*i*	75.54	71.24	71.30	1570*i*
TS11	46.32	44.23	44.18	998*i*	52.73	50.60	50.55	1027*i*
TS12	28.39	26.73	26.79	780*i*	31.86	30.21	30.33	779*i*
TS13	46.77	44.60	44.68	729*i*	49.77	47.60	47.72	741*i*

between amine hydrogen atoms and the H atom located on one of the triazole N atoms.

The theoretical results concerning the energetics of the AT amino forms in the gas phase are in disagreement with the experimental X-ray structure studied by Starova et al. [30]. These authors reported the 2-AT form with the annular H-atom attached to the N2 atom of the ring to be present in the AT crystal while 1-AT does not occur in the solid state. The influence of the environment on the stability order of the AT amino forms will be further considered in Section 3.4.

The gas phase structure of 2-AT determined at B3LYP/MP2 levels with the 6-311++G(2d,2p) basis set and the experimental X-ray data are in good agreement as concerns bond distance between heavy atoms and the majority of the bond angles and dihedral angles with the largest variation of 3%. There are significant discrepancies between experimental and theoretically predicted values for those angles and dihedral angles which involve hydrogen atoms. However, it is difficult to compare these parameters since it is known that the coordinates of hydrogen atoms are not precisely determined by X-ray diffraction measurements.

3.1.2. Annular tautomerism and interconversion pathways of the annular tautomers

Fig. 3 shows the ZPE corrected potential energy diagram for the annular tautomerisation of the amino forms of AT. The most stable 1-AT may izomerize to 2-AT by a direct 1,2-hydrogen transfer between two adjacent nitrogen atoms via the TS1 transition state

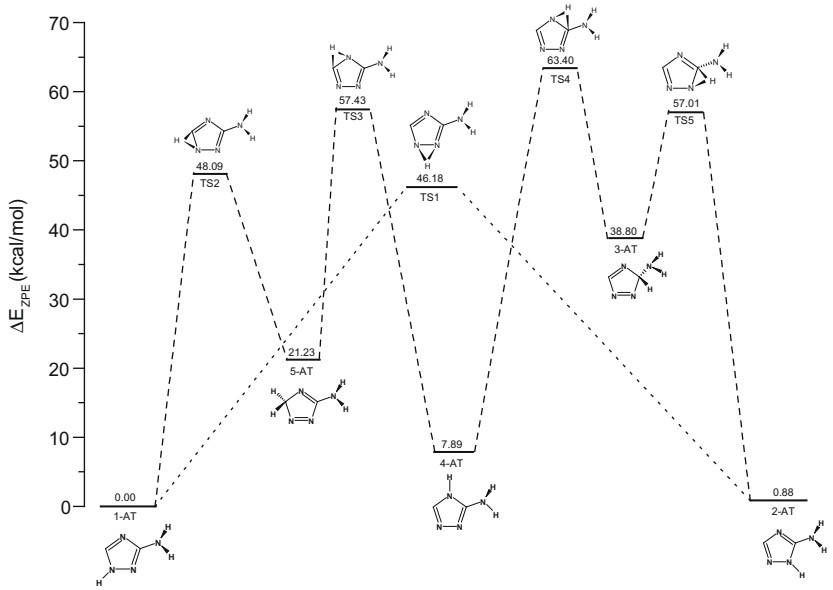

Fig. 3. B3LYP/6-311++G(2d,2p) potential energy diagram for the annular tautomerisations.

with the energy barrier of 46.18/45.20 kcal/mol. TS1 is characterized by a strongly elongated N1–N2 bond of 1.504/1.492 Å as compared with 1.367/1.356 Å and 1.372/1.360 Å in 1-AT and 2-AT, respectively. The key H7 atom takes the intermediate position between the N1 and N2 atoms and is situated out of the ring plane at the same side as the H atoms of the amino group.

Two other annular tautomerisations: 1-AT ↔ 4-AT and 2-AT ↔ 4-AT require two subsequent 1,2-hydrogen shifts leading to the intermediate products: 5-amino-*3H*-1,2,4-triazole (5-AT) or 3-amino-*3H*-1,2,4-triazole (3-AT), respectively. Both 1-AT ↔ 5-AT ↔ 4-AT and 2-AT ↔ 3-AT ↔ 4-AT processes proceed via two different high energy transition states (TS2, TS3 and TS4, TS5, respectively) lying more than 48 kcal/mol above the global minimum. All four transition states involve elongation of one C–N bond of the triazole ring and location of the transferring hydrogen atom out of the ring plane. As shown in Table 3 these transition states are characterized by relatively high imaginary frequency with the reaction coordinate involving H atom motion between two available positions.

3.1.3. Amino–imino tautomers and pathways of the amino–imino isomerization

The present calculations reveal the existence of three stable imino forms denoted as 1,2-ATIc, 2,4-ATIc and 1,4-ATIc characterized by different positions of two N–H bonds in the triazole ring and the imino N–H group in cis configuration relative to the N4 atom. Each of these imino forms has its isomer of slightly different energy with the trans conformation of the imino group relative to the N4 atom (1,2-ATIt, 2,4-ATIt and 1,4-ATIt, respectively).

Fig. 4a and b shows the ZPE corrected potential energy diagrams for the amino–imino isomerization pathways for the studied molecule. The 1,2-ATIc form may be obtained directly from the most stable 1-AT species through a high energy transition state TS6 characterized by a product-like structure with the N1–H7 bond tilted out from the ring plane and one of the amino group H atoms positioned close to the N2 ring atom, with the H···N2 distance equal to 1.29/1.27 Å. Similar pathways are expected for the 2-AT and 4-AT amino forms. These species may izomerize in one step processes via TS7 or TS8 transition states to form the 2,4-ATIt or

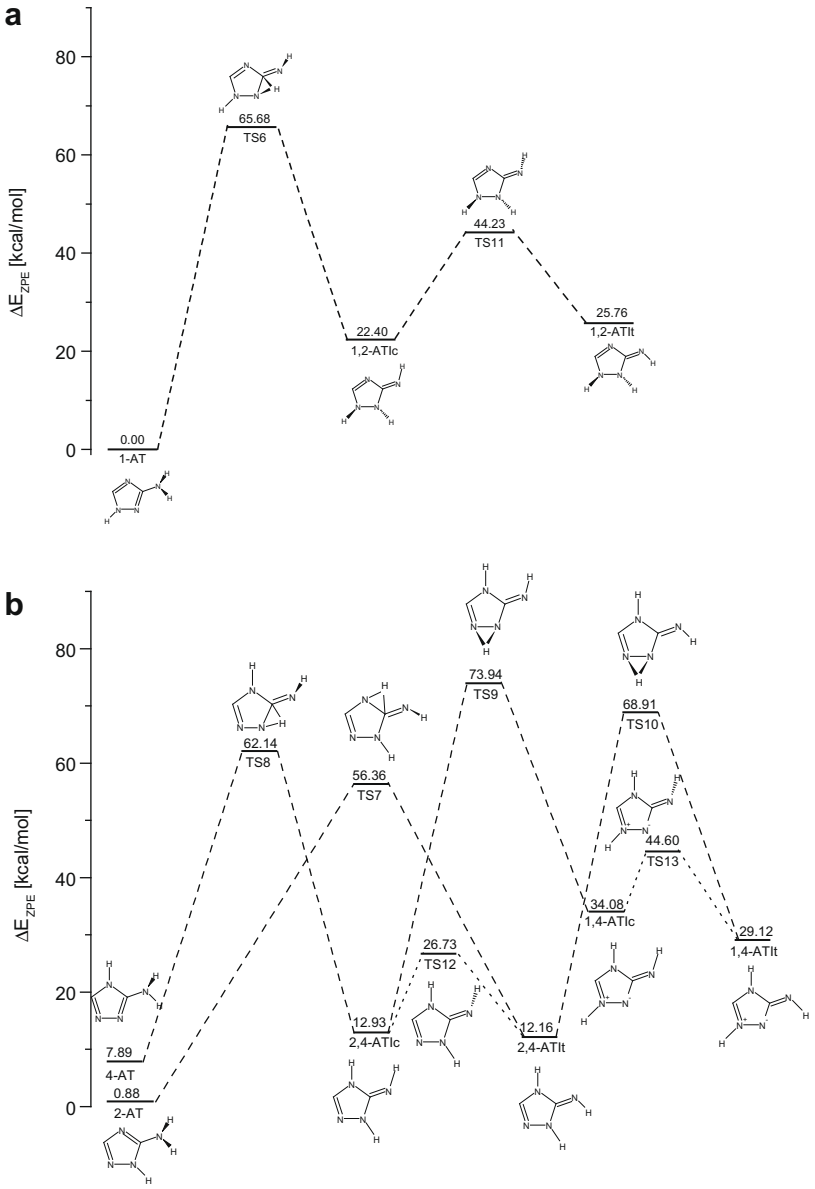

Fig. 4. B3LYP/6-311++G(2d,2p) potential energy diagram for the amino–imino isomerizations.

2,4-ATIc imino forms, respectively which differ by the position (trans or cis) of the N6–H imino group with respect to the N4 atom. The least stable imino forms (1,4-ATIc, 1,4-ATIt) cannot be directly obtained from either of three amino forms. However, as can be seen from Fig. 4b two step route is possible involving the amino–imino isomerization of the 2-AT or 4-AT as a first step through TS7 or TS8 and next an annular isomerization through TS9 or TS10 transition states to form 1,4-ATIc, 1,4-ATIt, respectively.

3.1.4. Cis–trans isomerizations between the imino-forms of AT

As it was already mentioned each of three imino forms may assume either cis (1,2-ATIc, 2,4-ATIc and 1,4-ATIc) or trans (1,2-ATIt, 2,4-ATIt and 1,4-ATIt) conformation with the N4C3N6H dihedral angle of 0.00° or 180.0°, respectively. The cis conformer is more stable for 1,2-ATI while the trans conformer has lower energy for the 2,4-ATI and 1,4-ATI species. The present calculations also reveal that the interconversions between cis and trans forms are possible with the relatively high activation energies of 14–24 kcal/mol. These reactions proceed through the TS11, TS12 and TS13 transition states characterized by the N4C3N6H dihedral angle of ca. 90°.

3.2. Population of the AT conformers

The relative abundance of the possible AT conformers was calculated using equation: $\Delta G = -RT\ln K$, where ΔG denotes the difference between Gibbs free energy for given two isomeric forms and K is the equilibrium constant for these species. The obtained abundance values with the degeneracy factor included are gathered in the last column of Table 2. The abundance of the two most stable species, 1-AT and 2-AT, equals 79.4% and 20.6% at 298 K and it changes very slightly at the experimental sublimation temperature of 333 K (78.9% and 21.1%). The remaining structures have a negligible total population and are expected to be of no importance in relation to the experimental spectra.

3.3. Matrix Isolation Infrared spectra and their comparison to the theoretical predictions

Positions of the bands observed for the 1-AT conformer in solid argon together with the frequencies predicted by the calculations are given in Table 4. The analogues data for the 2-AT form are presented in Table S2 (Supplementary material). The proposed assignment of the IR bands, also included in Table 4 and S2, is based on the analysis of the theoretically predicted spectra and the potential energy distribution (PED) matrices obtained for the 1-AT and 2-AT conformers (Tables S3–S6 in Supplementary material).

The key regions of the IR spectrum of AT isolated in an argon matrix deposited at 10 K are presented in Fig. 5 (upper traces). Analysis of the experimental spectrum allows, in agreement with the theoretical predictions, to exclude the presence of any of the AT imino forms. All three imino forms (1,2-ATI, 2,4-ATI and 1,4-ATI) are not only much higher in energy (compare Table 2) but are also expected to show a very intense absorption due to the ν C=N stretching mode of the imino group between 1640 and 1680 cm^{-1} (see Table S7 in Supplementary material). No trace of any bands in this range was found in our spectra. Thus, to interpret the experimental spectra it was accepted that only amino forms are present in the studied matrices. Moreover, a satisfying reproduction of the experimental spectrum was obtained when two most stable amino forms (1-AT and 2-AT) were taken into account with the gas phase abundance ratio. This suggests that the equilibrium gas phase mixture of the AT isomers is frozen in an argon matrix environment. There are no meaningful differences observed in the spectra when the deposition temperature is changed between 10 and 22 K. Thus, a conformation cooling phenomenon [32,34]

Table 4
Observed and calculated vibrational frequencies (cm^{-1}) and intensities (km/mol) of 1-AT.

B3LYP			MP2		Ar matrix[b]	Assignment[d]
Harmonic	Anharmonic	Scaled[a]	Harmonic	Scaled		
3682 (38)	3517	3518	3709 (39)	3544	3520 (0.21)[c]	$\nu_{as}NH_2$
3675 (84)	3499	3511	3690 (107)	3526	3507 (0.41)	νNH
3581 (28)	3430	3422	3600 (26)	3440	3425 (0.16)	$\nu_s NH_2$
3252 (2)	3137	3107	3297 (2)	3150	–	νCH
1649 (190)	1613	1612	1652 (135)	1615	1609 (1.00)	δNH_2
1585 (149)	1546	1549	1563 (164)	1528	1551, 1550 (0.40)	νCN_{ring}
1515 (36)	1482	1481	1512 (24)	1478	1487, 1493 (0.11)	νC–NH_2
1475 (35)	1429	1442	1489 (18)	1455	1444 (0.14)	νCN_{ring} + δNH
1380 (51)	1345	1349	1386 (35)	1355	1354 (0.27)	νCN_{ring}
1295 (8)	1270	1266	1298 (5)	1269	1268 (0.06)	δCH
1190 (4)	1156	1163	1190 (8)	1163	1167 (0.05)	νCN_{ring} + νNN_{ring}
1107 (10)	1092	1082	1122 (9)	1097	1102 (0.07) 1054* (0.05)	rNH_2
1062 (50)	1027	1038	1093 (40)	1068	1030 (0.05)	νNN_{ring} + δNH_2
1007 (1)	992	984	1001 (0)	978	993* (0.06)	δNNC_{ring} + νCN_{ring}
991 (3)	975	969	990 (4)	968	974,978* (0.04) 949* (0.10)	δNNC_{ring} + δNCN_{ring}
854 (16)	848	835	802(26)	784	846 (0.10) 793* (0.04)	τCH
783 (40)	752	765	786 (96)	768	758 (0.08)	τNCN_{ring} + τNH_2
740 (2)	730	723	736 (4)	719	740 (0.01)	δNCN_{ring} + νC–NH_2
658 (12)	643	643	677 (119)	662	645 (0.01)	γ_{ring}
603 (223)	467	589	671(54)	656	478 (0.37)	τNH_2
446 (94)	465	436	503 (85)	492	434 (0.22)	τNH
420 (4)	418	411	414 (3)	405	–	$\delta NCNH_2$
325 (30)	325	318	318 (27)	311	–	τ_{ring}
291 (28)	294	284	262 (33)	256	–	γNH_2

[a] For values of the scaling factors see Section 2.1.
[b] Doublets observed are due to the matrix site effect; for explanation of the origin of bands marked with an asterisk see the text.
[c] For experiment the relative integrated intensities are given in parentheses.
[d] Abbreviations are as follows: ν – bond stretching, δ – bending, deformation in plane, γ – twisting, τ – torsion, out-of-plane bending, r – rocking.

does not appear in the present case. Given the high value of the energy barrier calculated for the 1-AT ↔ 2-AT conversion through the transition state T1 of 46.18/45.20 kcal/mol (see Table 3) this conclusion is fully justified.

The spectrum resulting from adding the theoretically (B3LYP) predicted IR spectra of the 1-AT and 2-AT conformers scaled by their calculated abundance at the sublimation temperature (333 K) is also shown in Fig. 5 (middle trace). The calculated frequencies were scaled by the scaling factors as described in Section 2.1 to correct for the overestimation of the theoretical vibrational frequencies.

The 3550–3400 cm^{-1} region in the spectra is characteristic of the stretching vibrations of the NH_2 and NH groups in both 1-AT and 2-AT and their assignment is straightforward. In turn, the region below 1650 cm^{-1} is more difficult for analysis since it reflects, in agreement with the PED matrices obtained for both 1-AT and 2-AT, the presence of deformation modes of the NH_2 and NH groups as well as strongly coupled triazole ring stretching and deformation modes. Generally, as it is seen from Fig. 5 and Table 4, the agreement between the B3LYP spectra and the experimental argon matrix results is good. Two points, however, require further comment. First concerns the position of the out of plane deformation mode of the NH_2 group in 1-AT. The B3LYP scaled frequency for this mode equals 589 cm^{-1} that is much too high as compared to the experimental value of 478 cm^{-1}. Better agreement is found when one takes the calculated anharmonic frequency into account (467 cm^{-1}) as shown by a dashed line in Fig. 5. Second point is the presence of several weak bands marked with asterisk in Table 4

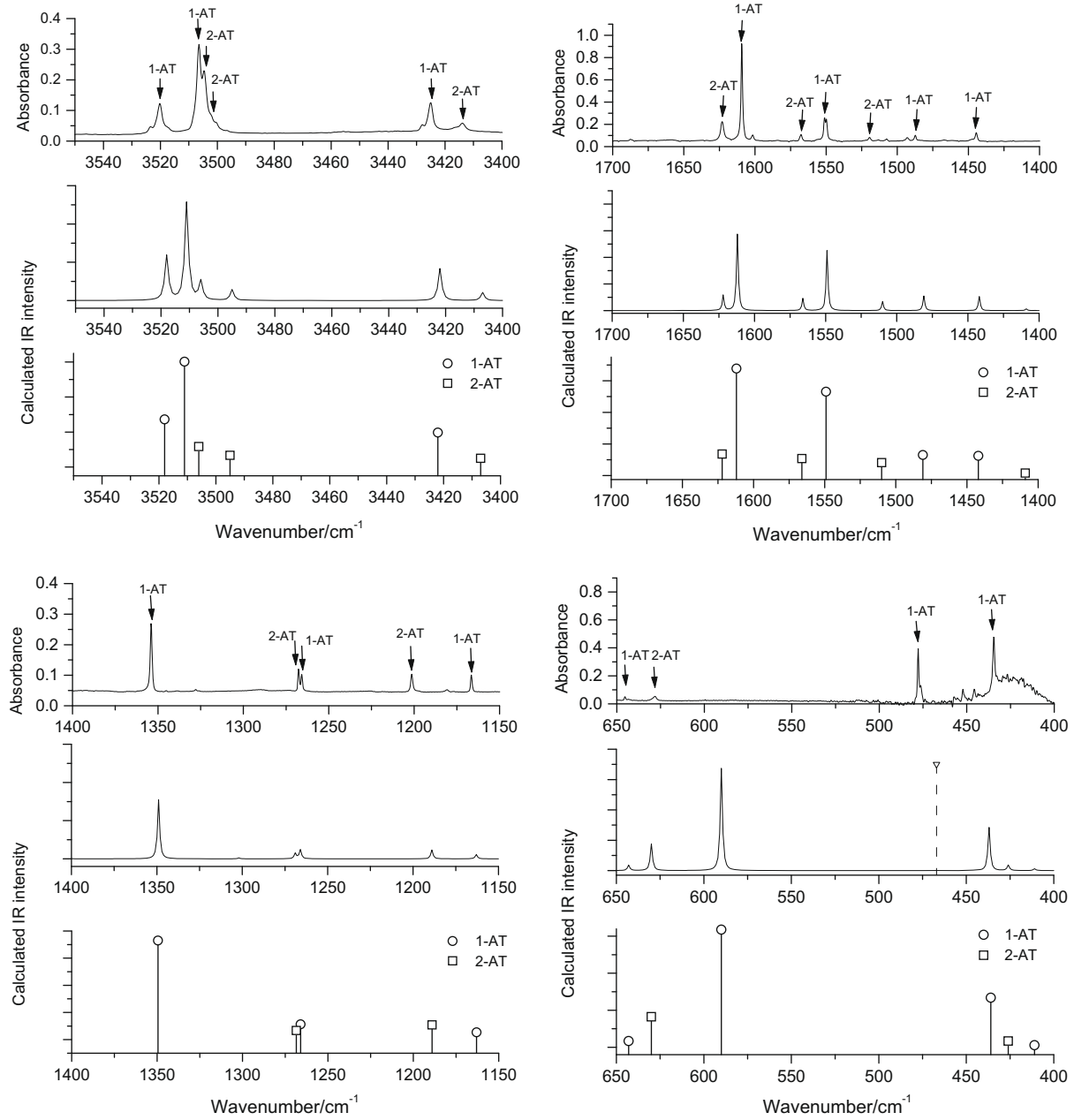

Fig. 5. The selected regions of AT spectra. *Top frame*: infrared spectrum of AT isolated in an argon matrix at 10 K. *Middle frame*: Sum spectrum obtained by adding the B3LYP/6-311++G(2d,2p) spectra of 1-AT and 2-AT weighted by their respective abundances (79% and 21%). The theoretical spectra were simulated using Lorentzian functions centered at the calculated frequencies scaled as described in Section 2.1 and with the bandwidth-at-half-height equal to 1.5 cm^{-1}. *Bottom frame:* Spectra of 1-AT and 2-AT calculated at B3LYP/6-311++G(2d,2p) level and scaled by the same scaling factors as for the middle fram.

Table 5
Calculated ZPE corrected energy difference ΔE (kcal/mol) and dipole moment μ(D) for 1-AT and 2-AT at the B3LYP/6–311++G(2d,2p) level for various values of the dielectric constant ε.

Solvent	1-AT		2-AT	
	ΔE	μ	ΔE	μ
Gas phase	0.00	2.00	0.88	3.65
Ar (ε = 1.43)	0.00	2.16	0.66	4.00
CCl_4 (ε = 2.23)	0.00	2.35	0.39	4.39
CH_2Cl_2 (ε = 8.93)	0.00	2.77	−0.28	5.23
Water (ε = 78.39)	0.00	2.96	−0.60	5.58

which, according to the calculations, are not expected to appear (see Table S1 in Supplementary material). Possible explanations are a slight deformation of the triazole ring in matrix cage that may increase a transition dipole moment of the particular ring modes and/or intensity enhancement of some overtones or combination bands by Fermi resonance interactions.

3.4. Solvation effects

The performed calculations revealed that in the gas phase 1-AT is the most stable tautomer and that 2-AT is less stable by 0.89/1.02 kcal/mol. These results are in disagreement with the experimental X-ray structure where only 2-AT is present [30]. This discrepancy is similar to that what was previously observed for tetrazole [38,39]. To investigate the effects of environment polarity on the structure and energetics of two most stable AT conformers the Onsager reaction field model at the B3LYP/6-311++G(2d,2p) level was applied. Four solvents were considered with the following dielectric constants: argon (ε = 1.43), carbon tetrachloride (ε = 2.23), dichloromethane (ε = 8.93) and water (ε = 78.39). The obtained relative energies and dipole moments are given in Table 5. From the analysis of the results it appears that 1-AT is more stable in less polar solvents while 2-AT becomes more stable in CH_2Cl_2 and H_2O. The latter observation explains the presence of the 2-AT tautomer in the crystalline phase [30]. The effects of varying the dielectric constant on the geometry of 1-AT and 2-AT are illustrated in Table S8 (Supplementary material) where parameters having the largest variations in at least one conformer with the changing ε are gathered. As expected, the 2-AT molecule interacts stronger with the environment displaying larger modifications of the geometrical parameters than the 1-AT molecule does. Table S8 shows that the internal parameters most influenced by the solvents in both isomers are the annular N–H bond with the absolute percentage difference in water relative to the gas phase of 1.79% and the θ(H9N6H10) angle (ca. 1%). There are also several parameters which are apparently more solvent-sensitive in the 2-AT conformer than in 1-AT. Among them are the R(C3–N4) and R(C3–N6) bonds (1.14% and 1.01%, respectively) and θ(C3N6H9) angle (2.06%). There are also significant modifications in those dihedral angles which describe the orientation of the amino group relative to the ring. For example, the ϕ(N4C3N6H9) and ϕ(N4C3N6H10) in 2-AT vary, respectively, from 12.5° to 23.2° and from 142.0° to 157.0° with the dielectric constant changes from ε = 1 to ε = 78.4. These results indicate both energetic and geometric changes due to solvation similar to those reported for a pair of annular conformers of 3-amino-5-nitro-1,2,4-triazole [3].

4. Concluding remarks

1. Eleven minima and thirteen transition states were located on the singlet PES for the 3-amino-1,2,4-triazole at the B3LYP/6-311++G(2d,2p) and MP2/6-311++G(2d,2p) levels. All available isomerization pathways were identified and discussed.
2. 3-amino-1,2,4-*1H*-triazole (1-AT) is the most stable structure in the gas phase and 3-amino-1,2,4-*2H*-triazole (2-AT) is only slightly less stable by ca. 1 kcal/mol.
3. The remaining isomers are much higher in energy and according to the calculated abundance values only 1-AT and 2-AT are expected to appear in the gas phase.
4. The experimental FTIR spectra are well reproduced by the spectrum resulting from adding B3LYP predicted spectra of 1-AT and 2-AT scaled by their calculated abundance. The presented results allow unequivocal identification and characterization of the two tautomers isolated in an argon matrix.
5. The assignment of the experimental IR bands could be done based on the analysis of the theoretically predicted spectra and the potential energy distribution (PED) matrices obtained for the 1-AT and 2-AT conformers.
6. The performed studies reveal that conformational cooling did not take place in the studied matrices. This observation is consistent with the predicted high energy barrier of ca. 45 kcal/mol for a direct 1,2-hydrogen transfer between 1-AT and 2-AT species.
7. The results of geometry optimization obtained when solvent effects are considered suggest that in non-polar solvents (ε = 1.46 and 2.23), similarly as in the gas phase, the most stable species is 1-AT while in polar solvents the most stable is 2-AT tautomer in agreement with X-ray diffraction data obtained for the crystalline sample.
8. The results of this study allow for better understanding of the structural, energetic and spectroscopic properties of AT isomers as well as differences among them.

Acknowledgement

A grant of computer time from the Wrocław Center for Networking and Supercomputing is gratefully acknowledged.

Appendix A. Supplementary material

The selected calculated geometric parameters for less stable conformers (Table S1), observed and calculated frequencies and intensities of 2-AT (Table S2), definition of internal coordinates and results of normal coordinate analysis for 1-AT and 2-AT (Tables S3-S6), the B3LYP calculated harmonic frequencies and intensities for less stable isomers (Table S7), influence of dielectric constant on the selected geometric parameters of 1-AT and 2-AT (Table S8) and the 1100–750 cm^{-1} region of the AT spectra (Fig.S1). This material is available free of charge via the Internet at http://pubs.acs.org. Supplementary data associated with this article can be found, in the online version, at doi:10.1016/j.cplett.2009.03.079.

References

[1] A.S. Lyakhov, A.N. Vorobiov, P.N. Gaponik, L.S. Ivashkevich, V.E. Matulis, O.A. Ivashkevich, Acta Cryst. C 59 (2003) o690.
[2] L-H. Jia, Z-L. Liu, W. Liu, Acta Cryst. E 63 (2007) o2766.
[3] D.C. Sorescu, C.M. Bennett, D.L. Thompson, J. Phys. A 102 (1998) 10348.
[4] J.-L.M. Abboud et al., Eur. J. Org. Chem. (2001) 3013.
[5] W.P. Ozimiński, J.Cz. Dobrowolski, A.P. Mazurek, J. Mol. Struct. (Theochem) 680 (2004) 107.
[6] M.H. Palmer, D. Christem, J. Mol. Struct. 705 (2004) 177.
[7] V. Jiménez, J.B. Alderete, J. Mol. Struct. (Theochem) 775 (2006) 1.
[8] A.A. El-Azhary, H.U. Suter, J. Kubelka, J. Phys. Chem. A 102 (1998) 620.
[9] G. Da Silva, E.E. Moore, J.W. Bozzelli, J. Phys. Chem. A 110 (2006) 13979.
[10] V.E. Matulis, O.A. Ivashkevich, P.N. Gaponik, P.D. Elkind, G.T. Sukhanov, A.B. Bazyleva, D.H. Zaitsau, J. Mol. Struct. 854 (2008) 18.
[11] F. Billes, H. Endrédi, G. Keresztury, J. Mol. Struct. 530 (2000) 183.
[12] V. Krishnakumar, R.J. Xavier, Spectrochim. Acta A 60 (2004) 709.
[13] S. Zaza, F. Guedira, S. Zaydoun, M. Saidi Idrissi, A. Lautie, F. Romain, Can. J. Anal. Sci. Spectosc. 49 (2004) 15.

[14] V. Krishnakumar, G. Keresztury, T. Sundius, R.J. Xavier, Spectrochim. Acta A 61 (2005) 261.
[15] S. Thomas, N. Biswas, S. Venkateswaran, S. Kapoor, R. D'Cunha, T. Mukherjee, Chem. Phys. Lett. 402 (2005) 361.
[16] M. Kiszka, I.R. Dunkin, J. Gębicki, H. Wang, J. Wirz, J. Chem. Soc., Perkin Trans. 2 (2000) 2420.
[17] P.J. Sánchez-Soto, E. Morillo, J.L. Pérez-Rodríguez, C. Real, J. Therm. Anal. 45 (1995) 1189.
[18] J. Li, T.A. Litzinger, Thermochim. Acta 454 (2007) 116.
[19] M. Badea, R. Olar, D. Marinescu, G. Vasile, J. Therm. Anal. Calorim. 92 (2008) 209.
[20] N.V. Kumar, U.C. Mashelkar, Heterocycl. Commun. 13 (2007) 211.
[21] I. Perez-Castro, O. Caamano, F. Fernandez, M.D. Garcia, C. Lopez, E. De Clercq, Org. Biomol. Chem. 5 (2007) 3805.
[22] O. Bekircarcan, H. Bektas, Molecules 11 (2006) 469.
[23] J.G. Haasnoot, Coord. Chem. Rev. 200–202 (2000) 131.
[24] W. Li, H-P. Jia, Z-F. Ju, J. Zhang, Cryst. Growth Des. 6 (2006) 2136.
[25] Z. Chen, X. Li, F. Liang, J. Solid State Chem. 181 (2008) 2078.
[26] Y-Y. Lin, Y-B. Zhang, J-P. Zhang, X-M. Chen, Cryst. Growth Des. 8 (2008) 3673.
[27] P.J. van Koningsbruggen, Top. Curr. Chem. 233 (2004) 123.
[28] Y. Garcia, V. Niel, M.C. Mun?z, J.A. Real, Top. Curr. Chem. 233 (2004) 229.
[29] R. Bronisz, Inorg. Chem. 44 (2005) 4463.
[30] G.L. Starova, O.V. Frank-Kamenetskaya, V.V. Makarshii, V.A. Lopirev, Kristallografiya 23 (1978) 849.
[31] A. Kaczor, I.D. Reva, L.M. Proniewicz, R. Fausto, J. Phys. Chem. A 111 (2007) 2957.
[32] I.D. Reva, A.J. Lopes Jesus, M.T.S. Rosado, R. Fausto, M.E. Eusébio, J.S. Redinha, Phys. Chem. Chem. Phys. 8 (2006) 5339.
[33] A. Olbert-Majkut, M. Wierzejewska, J. Phys. Chem. A 112 (2008) 5691.
[34] Y. Haas, U. Samuni, Prog. React. Kinet. 23 (1998) 211.
[35] M.J. Frisch et al., Gaussian 03, Revision C.02, Gaussian, Inc., Wallingford, CT, 2004.
[36] J.M.L. Martin, C. Van Alsenoy, GAR2PED, University of Antwerp, Antwerpen, Belgium, 1995.
[37] K. Irikura, National Institute of Standards and Technology, Gaithesburg, MD 20899, USA, 1995.
[38] S.C.S. Bugalho, E.M.S. Maçôas, M.L.S. Cristiano, R. Fausto, Phys. Chem. Chem. Phys. 3 (2001) 3541.
[39] R. Goddard, O. Heinemann, C. Krüger, Acta Cryst. C 53 (1997) 590.